
GENERATING CLINICALLY REALISTIC EHR DATA VIA A HIERARCHY- AND SEMANTICS-GUIDED TRANSFORMER

A PREPRINT (UNDER REVIEW)

Guanglin Zhou^{1,*} and Sebastiano Barbieri¹

¹The University of Queensland, Brisbane, Australia

*Corresponding author: guanglin.zhou@uq.edu.au

ABSTRACT

Generating realistic synthetic electronic health records (EHRs) holds tremendous promise for accelerating healthcare research, facilitating AI model development and enhancing patient privacy. However, existing generative methods typically treat EHRs as flat sequences of discrete medical codes. This approach overlooks two critical aspects: the inherent hierarchical organization of clinical coding systems and the rich semantic context provided by code descriptions. Consequently, synthetic patient sequences often lack high clinical fidelity and have limited utility in downstream clinical tasks. In this paper, we propose the Hierarchy- and Semantics-Guided Transformer (HiSGT), a novel framework that leverages both hierarchical and semantic information for the generative process. HiSGT constructs a hierarchical graph to encode parent-child and sibling relationships among clinical codes and employs a graph neural network to derive hierarchy-aware embeddings. These are then fused with semantic embeddings extracted from a pre-trained clinical language model (e.g., ClinicalBERT), enabling the Transformer-based generator to more accurately model the nuanced clinical patterns inherent in real EHRs. Extensive experiments on the MIMIC-III and MIMIC-IV datasets demonstrate that HiSGT significantly improves the statistical alignment of synthetic data with real patient records, as well as supports robust downstream applications such as chronic disease classification. Our evaluations, based on fidelity, utility, and privacy metrics, indicate that HiSGT not only enhances the quality of synthetic EHR data but also preserves patient privacy. By addressing the limitations of conventional raw code-based generative models, HiSGT represents a significant step toward clinically high-fidelity synthetic data generation and a general paradigm suitable for interpretable medical code representation, offering valuable applications in data augmentation and privacy-preserving healthcare analytics.

Keywords Electronic health records · Synthetic data generation · Hierarchy and semantics-guided · Generative transformer

1 Introduction

Electronic Health Records (EHRs) are a cornerstone of modern healthcare, playing a pivotal role in patient care, clinical decision-making, and medical research [Jha et al., 2009, Cowie et al., 2017, Xiao and Sun, 2021, Xiao et al., 2018]. Despite their importance, strict regulations surrounding privacy and data confidentiality have made it challenging to share and utilize EHR data at scale [Johnson et al., 2016, 2023]. As a result, there is growing interest in **synthetic EHR data generation**, a paradigm that aims to produce clinically realistic datasets mimicking the distributional properties of real EHRs while protecting sensitive patient information [Gonzales et al., 2023, McDuff et al., 2023, van Breugel et al., 2024, Ghosheh et al., 2024]. By balancing privacy preservation and data utility, synthetic EHRs hold the promise of accelerating model benchmarking, enabling data augmentation, and facilitating collaborative research.

Recent advances in generative models have spurred significant progress in synthetic EHR data generation. Many approaches use Generative Adversarial Networks (GANs) [Choi et al., 2017, Zhang et al., 2021, Torfi and Fox, 2020, Cui et al., 2020, Zhang et al., 2020, Rashidian et al., 2020, Kuo et al., 2022] and Variational AutoEncoders (VAEs) [Biswal

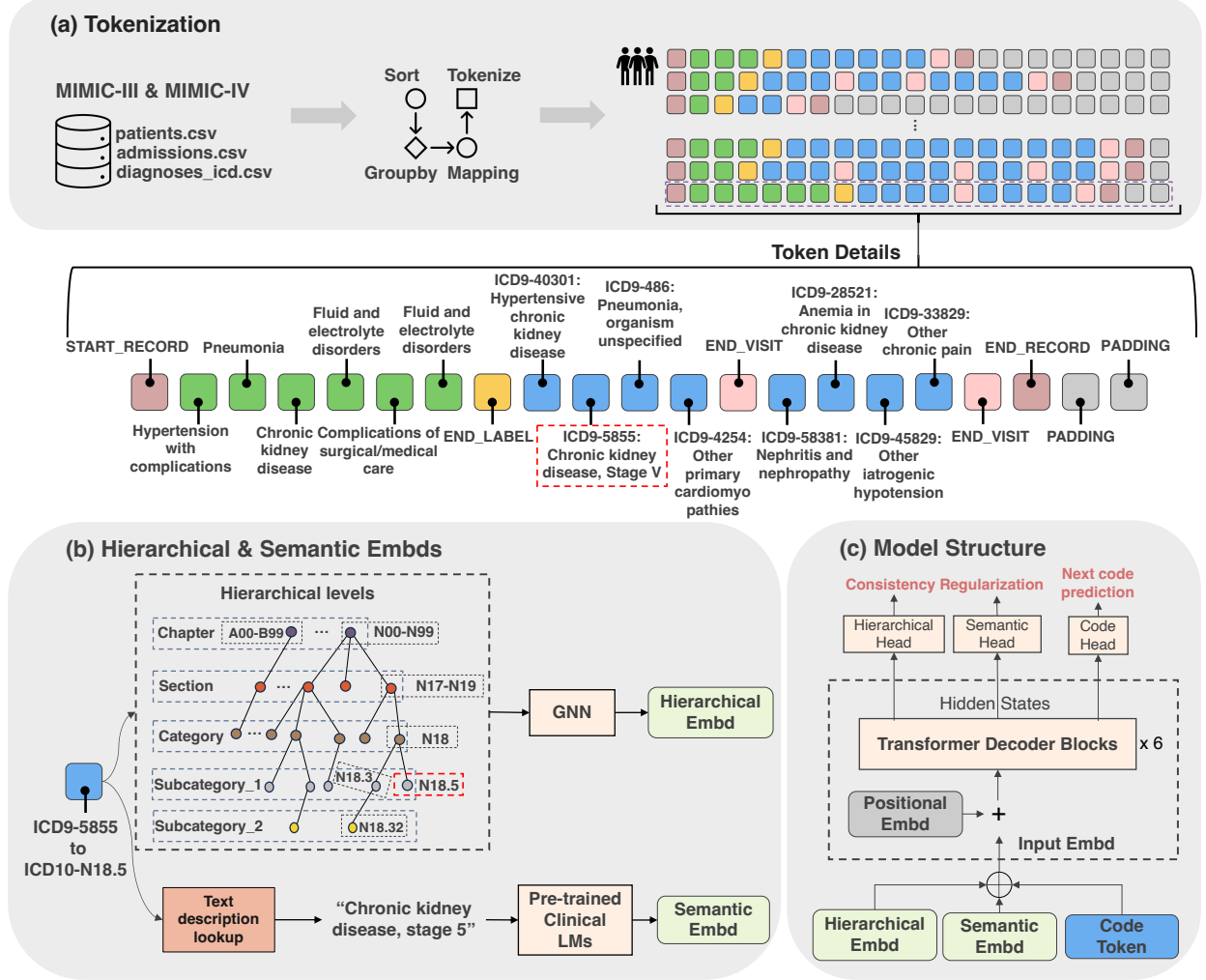


Figure 1: Overview of HiSGT for Synthetic EHR Generation. (a) Tokenization: We extract structured patient records from the MIMIC-III and MIMIC-IV datasets, and process hospital admissions and diagnosis codes. The tokenization process encodes patient timelines into structured sequences, strictly following the format: {START_RECORD, phenotype label tokens, END_LABEL, event tokens per visit, END_VISIT, ..., END_RECORD, PADDING}. (b) Hierarchical & Semantic Embeddings: Medical codes (e.g., ‘N18.5’) are enriched with hierarchical embeddings from a constructed ICD-based graph and semantic embeddings from a pre-trained clinical language model (LM), e.g., ClinicalBERT. The GNN-derived hierarchical embeddings capture multi-level taxonomic relationships, while ClinicalBERT encodes text descriptions. (c) Model Structure: HiSGT integrates hierarchical and semantic embeddings into Transformer-based decoder blocks. Three prediction heads—hierarchical, semantic, and next-code prediction—jointly optimize the model. During inference, HiSGT autoregressively generates synthetic patient records, starting from the first token START_RECORD and sequentially predicting phenotype labels, medical visit/events until reaching END_RECORD.

et al., 2021]. Other methods have drawn on the Transformer architecture [Vaswani et al., 2017] to capture long-range dependencies in clinical sequences. In these models, medical codes and clinical events are typically treated as discrete tokens, with a next-token prediction objective used to model the sequential structure of EHR data [Theodorou et al., 2023, Kraljevic et al., 2024, Pang et al., 2024, Renc et al., 2024]. However, they overlook the rich semantic information embedded in clinical code descriptions and the inherent hierarchical relationships in clinical coding systems. Consequently, the synthesized patient sequences frequently lack high clinical fidelity, which limits the utility of the generated synthetic EHR data. In particular, two major research gaps remain.

First, medical coding systems such as the International Classification of Diseases (ICD) [Organization et al., 1978] are organized hierarchically, with codes exhibiting parent–child and sibling relationships that reflect key clinical knowledge. For example, in ICD-10, the code ‘E11’ (Type 2 diabetes mellitus) serves as a parent for ‘E11.6’ (type 2 diabetes mellitus

with other specified complications) and as an ancestor for ‘E11.65’ (Type 2 diabetes mellitus with hyperglycemia), while sibling codes such as ‘E11.65’ and ‘E11.64’ (Type 2 diabetes mellitus with hypoglycemia) capture different diabetes complications at a more granular level. In clinical practice, a patient may first be diagnosed at a coarse level with ‘E11’ and later be assessed for specific complications (e.g., ‘E11.64’ or ‘E11.65’). *However, current generative models often treat each code as an isolated symbol, failing to leverage these multi-level taxonomic properties.* As a result, they may generate conflicting sibling codes that cannot clinically co-occur (e.g., ‘E11.64’ hypoglycemia and ‘E11.65’ hyperglycemia in the same visit) or neglect important subcodes. Second, each medical code is accompanied by a textual description that clarifies its clinical semantics and distinguishes between disease subtypes. For instance, ‘E11.65’ denotes ‘Type 2 diabetes mellitus with hyperglycemia’, while ‘Z13.6’ specifies ‘screening for cardiovascular disorders’. Such text descriptions are essential for determining the precise clinical focus of a patient’s visit. In practice, each patient’s visit to the hospital often centers on a primary diagnosis (or a small set of diagnoses) with additional procedures tailored to that theme until the patient’s condition is confirmed by the physician. Consequently, the codes assigned within a single visit tend to be semantically related, reflecting the shared focus on a particular disease process. *However, existing generative methods typically disregard these semantic descriptions and treat codes solely as discrete tokens.* Without leveraging the underlying semantics, these models may synthesize codes that are logically or clinically incompatible.

Beyond these challenges, EHR data are inherently high-dimensional and sparse. For example, datasets like MIMIC-III [Johnson et al., 2016] and MIMIC-IV [Johnson et al., 2023] contain thousands of unique diagnostic codes, many of which occur infrequently. This sparsity and high dimensionality pose challenges in capturing the statistical and clinical relationships among codes. Without incorporating additional information—such as textual descriptions or hierarchical structures—purely raw code-based methods struggle with these nuances. As a result, many generative approaches mitigate this issue by reducing data complexity, often through aggregating medical codes or removing rare codes [Theodorou et al., 2023]. Consequently, the generated synthetic patient sequences often exhibit low clinical fidelity, ultimately limiting their practical utility in real-world healthcare applications.

To address these limitations, we propose a novel framework called Hierarchy and Semantics-Guided Transformer (HiSGT), which integrates both hierarchical relationships and semantic information into the generative process. HiSGT begins by constructing a hierarchical graph to mirror the taxonomy of real coding systems such as ICD, preserving the parent–child and sibling relationships. This graph helps to encode and extract clinically coherent paths for every single code (e.g., from ‘E11.6’ to ‘E11.65’). A graph neural network (GNN) is then employed to learn hierarchy-aware embeddings that capture structured dependencies among medical codes. Additionally, HiSGT enriches each medical code with semantic embeddings derived from a pre-trained clinical language model (e.g. ClinicalBERT [Alsentzer et al., 2019]). These embeddings are consistent with their text description to help inject essential domain knowledge into the Transformer backbone. Thus, concepts like ‘Type 2 diabetes’ carry meaningful distinctions rather than being treated solely as a meaningless token. Finally, these refined embeddings are fed into a Transformer-based generative model to synthesize EHR data that are both semantically consistent and structurally coherent. Our work makes the following key contributions to the field of synthetic EHR generation: (1) we propose a novel framework that leverages both hierarchical graph representations and clinical semantic embeddings, as an approach to embed medical codes in general, to overcome the limitations of raw code-only generative methods; (2) we develop an enhanced Transformer model that integrates refined code representations, enabling the generation of synthetic EHRs with high clinical fidelity; (3) we demonstrate the effectiveness of HiSGT on two real-world EHR datasets, showing significant improvements in data quality, downstream task performance (e.g., disease classification), and privacy preservation.

2 Results

2.1 Fidelity Evaluation

To assess the clinical fidelity of synthetic EHR data, we employ four complementary metrics that assess the alignment between real and synthetic records at different levels of granularity, capturing both individual event distributions and their relationships within and across patient visits. First, we compute the **Unigram** score, which measures how well the generated data preserves the marginal distribution of individual medical events. For each event, we count its occurrences in both the real and synthetic datasets and compute the coefficient R^2 between the two frequency distributions. A higher R^2 value indicates that the generated data preserves the marginal distribution of real-world medical events. Beyond individual event distributions, we assess co-occurrence structures by computing the **Bigram** score, which captures the statistical dependencies between pairs of medical events within the same visit. This score reflects *intra-visit* coherence—an essential property of high-fidelity EHR synthesis, as medical events within a visit often exhibit strong correlations. Similarly, the sequential bigram score (**Seq Bigram**) extends this evaluation to *inter-visit* dependencies, quantifying how well the synthetic data captures longitudinal patterns by examining the transitions between medical codes across consecutive visits. Finally, we compute the dimension-wise correlation (**DimWise**). Unlike Unigram that

Table 1: **Performance on Fidelity Metrics.** The table reports the R^2 scores for four metrics—Unigram (marginal event distribution), Bigram (intra-visit co-occurrence), Seq Bigram (inter-visit transitions), and DimWise (dimension-wise correlation)—evaluated on both MIMIC-III and MIMIC-IV.

Methods	MIMIC-III				MIMIC-IV			
	Unigram	Bigram	Seq Bigram	DimWise	Unigram	Bigram	Seq Bigram	DimWise
LSTM	0.939	0.522	0.339	0.806	0.970	0.736	0.737	0.822
GPT	0.935	<u>0.858</u>	<u>0.811</u>	<u>0.940</u>	0.969	<u>0.935</u>	0.907	<u>0.957</u>
EVA	0.986	0.749	0.779	0.869	-	-	-	-
SynTEG	0.036	-2.562	-0.579	-0.052	0.909	0.733	0.630	0.735
HALO-Coarse	0.933	0.774	0.637	0.701	0.927	0.743	0.712	0.900
HALO	0.936	<u>0.867</u>	<u>0.869</u>	0.764	<u>0.973</u>	0.932	<u>0.924</u>	0.947
HiSGT (Ours)	<u>0.984</u>	0.949	0.879	0.976	0.989	0.967	0.948	0.989

only captures overall dataset-level frequency distributions, DimWise measures the per-patient probability distribution of medical codes between real and synthetic data. We first construct code probabilities matrices for real and synthetic datasets, where each row represents a patient and each column represents an ICD code. The elements of the matrix correspond to the relative frequency of each ICD code within a given patient’s sequence. Specifically, for a patient with n total medical codes, the probability of each code is computed by dividing its occurrence count by n . We then compute the mean probability of each ICD code across all patients, reducing the original patient-code matrix to a single probability vector per dataset. The coefficient of determination (R^2 score) is computed between these two vectors (one for real and one for synthetic data) as the final DimWise score.

The results in Table 1 provide evidence of HiSGT’s superior ability to synthesize clinically faithful EHR data. For the MIMIC-III dataset, HiSGT achieves an Unigram score of 0.984, closely approximating the real data’s marginal distribution. More importantly, the intra-visit Bigram score reaches 0.949—an 8.2% improvement over HALO’s 0.867—indicating that HiSGT more accurately captures the co-occurrence patterns of medical events within a visit. The sequential dependencies, as measured by the Seq Bigram score, are also better modeled by HiSGT (0.879 versus 0.869 for HALO), while the DimWise metric (0.976) further confirms its effectiveness in preserving dimension-level correlations. Similarly, on the MIMIC-IV dataset, HiSGT consistently outperforms competing methods by recording a Unigram score of 0.989, a Bigram score of 0.967, and a Seq Bigram score of 0.948, compared to HALO’s scores of 0.973, 0.932, and 0.924, respectively. The DimWise score for HiSGT reaches 0.989, reinforcing its capability to capture both the marginal distributions and the complex dependencies inherent in clinical data. These improvements underscore the importance of incorporating hierarchical and semantic structures in generating synthetic EHR data.

To further evaluate the fidelity of synthetic EHR data, we visualize the alignment between real and synthetic medical code distributions using a scatter plot in Figure 2. Each point represents a unique medical code or medical code pair, and its occurrence frequency in the synthetic dataset plotted against its corresponding frequency in real data. Ideally, all points should lie along the diagonal red line, indicating a perfect match between synthetic and real distributions. From the figure, we observe that HiSGT exhibits a significantly tighter clustering of points along the diagonal compared to baseline models, while baseline models such as LSTM, GPT, and SynTEG show greater dispersion. This visualization figure supports the results in Table 1, where HiSGT consistently outperforms competing methods on Unigram, Bigram, and Seq Bigram scores.

2.2 Utility Evaluation

To evaluate the clinical utility of synthetic EHR data, we conduct a disease classification experiment that assesses whether predictive models trained on synthetic clinical data can generalize to real-world patient records. This experiment follows the **Train on Synthetic, Test on Real (TSTR)** evaluation paradigm, where models are first trained on synthetic data and then evaluated on real patient outcomes. This methodology ensures that synthetic data captures meaningful clinical patterns that can support downstream predictive modeling tasks [Esteban et al., 2017]. In our setting, we adopt the phenotype classification task, considering 25 phenotypes, a widely used benchmark in clinical predictive modeling [Harutyunyan et al., 2019]. For real data, phenotype labels are assigned using a rule-based mapping from ICD diagnosis codes to phenotype categories, based on the HCUP Clinical Classifications Software (CCS) [Harutyunyan et al., 2019]. Each patient in the real dataset is assigned one or more phenotype labels based on their recorded ICD codes. For synthetic data, phenotype labels are first generated by the model and then used to conditionally generate

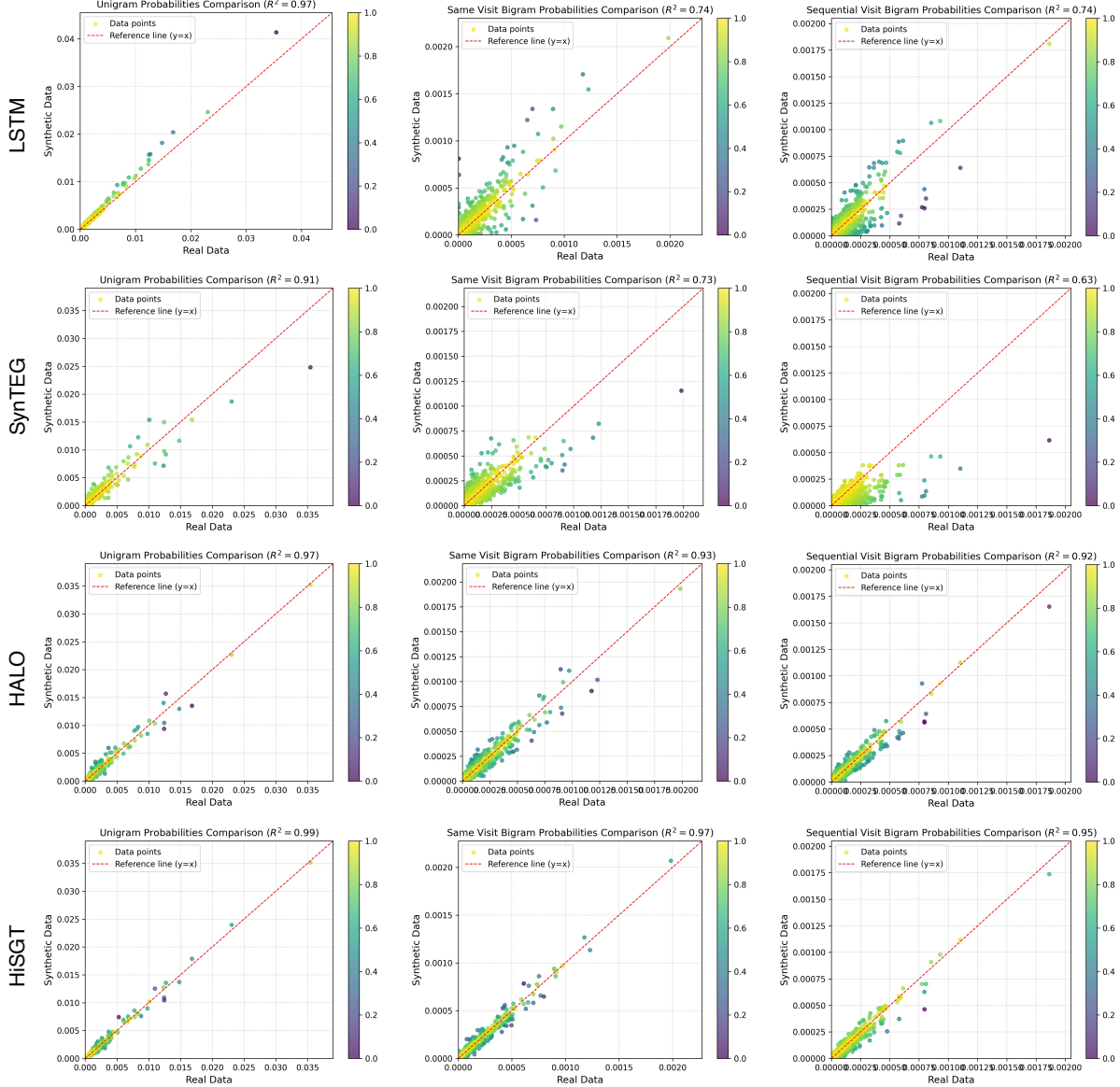


Figure 2: **Scatter plot of synthetic vs. real distributions for Unigram, Bigram and Seq Bigram on MIMIC-IV.** Each point represents a unique medical code or medical code pair, where its frequency in the synthetic dataset is plotted against its frequency in real data. The red diagonal line indicates perfect alignment with real distributions. HiSGT exhibits a tighter clustering along the diagonal compared to baselines, demonstrating superior fidelity in preserving real-world code distributions.

patient visit sequences containing medical codes, following the approach in [Esteban et al., 2017]. This conditional generation strategy ensures that patient trajectories are synthesized in a way that maintains meaningful associations between phenotype labels and clinical events. For the classification model, we employ a bi-directional LSTM classifier with a fully connected output layer [Theodorou et al., 2023]. For each dataset, we randomly extract 5,000 patient records for training, maintaining a balanced distribution of positive and negative labels for every single chronic disease category. Further, we reserve a separate validation set of 250 records for model selection and 500 real patient records as a held-out test set. Table 2 presents the classification results for various baseline models. We report accuracy, precision, recall, and F1-score, with standard deviations computed over the 25 phenotype labels. The performance of models trained on real data serves as an upper bound for comparison. Among synthetic data models, HiSGT consistently achieves the highest performance, surpassing HALO and other baseline methods in both MIMIC-III and MIMIC-IV datasets. These results highlight the effectiveness of our conditional generation strategy, demonstrating that HiSGT-generated patient

Table 2: **Performance on Phenotype Classification.** This table presents the results of the Train on Synthetic, Test on Real (TSTR) evaluation for phenotype classification. Models are trained on synthetic patient records and evaluated on real MIMIC-III and MIMIC-IV datasets. We report the average accuracy, precision, recall, and F1-score (with standard deviations) across 25 phenotype categories. Higher scores indicate better generalization to real-world patient data.

Methods	MIMIC-III				MIMIC-IV			
	Acc	Precision	Recall	F1-Score	Acc	Precision	Recall	F1-Score
Real Data	0.951±0.02	0.946±0.02	0.957±0.03	0.951±0.02	0.945±0.02	0.936±0.02	0.956±0.02	0.946±0.02
LSTM	0.493±0.06	0.480±0.12	0.673±0.26	0.538±0.17	0.545±0.10	0.534±0.15	0.580±0.18	0.546±0.14
GPT	0.885±0.04	0.862±0.05	0.919±0.05	0.889±0.04	0.883±0.05	0.864±0.05	0.912±0.05	0.887±0.04
EVA	0.500±0.07	0.470±0.15	0.636±0.26	0.526±0.17	-	-	-	-
SynTEG	0.515±0.03	0.605±0.17	0.680±0.38	0.513±0.22	0.563±0.08	0.622±0.11	0.558±0.26	0.533±0.12
HALO-Coarse	0.858±0.05	0.855±0.05	0.865±0.07	0.859±0.05	0.827±0.05	0.827±0.05	0.830±0.08	0.826±0.05
HALO	0.892±0.03	0.871±0.04	0.920±0.04	0.895±0.03	0.893±0.04	0.880±0.04	0.909±0.05	0.894±0.04
HiSGT (Ours)	0.898±0.04	0.878±0.05	0.927±0.05	0.901±0.04	0.905±0.04	0.888±0.03	0.929±0.04	0.907±0.04

trajectories retain the clinical coherence necessary for accurate phenotype classification. Table 3 provides a detailed breakdown of classification performance across different disease types (acute, chronic, and mixed). The macro-averaged accuracy and F1-score across each disease category offer insights into how well synthetic data generalizes across different clinical conditions. Across all disease types, HiSGT demonstrates superior performance over current SOTA method HALO.

2.3 Privacy Evaluation

In addition to ensuring high fidelity and utility, it is critical that synthetic EHR data do not compromise patient privacy [Giuffrè and Shung, 2023]. To this end, we evaluate the privacy protection of our synthetic data by simulating two common attacks: a membership inference attack (MIA) and an attribute inference attack (AIA). These attacks are designed to assess whether an adversary could either determine if a particular patient record was used during training or infer sensitive attributes from the synthetic records. Specifically, MIA tests whether an adversary can correctly classify a real patient record as having been used (or not used) during the synthetic data generation process. We construct an attack dataset by randomly sampling 500 records from the training set (labeled as positive) and 500 records from the test set (labeled as negative). For each record in this attack set, we compute the minimum Hamming distance to the synthetic dataset. By comparing each distance to the median distance of the entire attack set, records are classified as *members* (*positive*) if the distance is below the median and as *non-members* otherwise. An accuracy close to 50% indicates that the synthetic data do not leak membership information beyond what would be expected by random guessing. The AIA aims to determine whether sensitive attributes can be reliably predicted from the synthetic data. We transform both real and synthetic patient records by aggregating visit-level information and then select a set of common codes (derived from the most frequent 100 codes in the training data) to serve as a basis for inference. For each record, we compare the known label set with those of its nearest neighbors (based on a simple set-based distance) and predict additional codes via a majority vote. The performance of the attack is measured using an F1-score (AIA-F1), where lower scores indicate better privacy protection by the synthetic data. Table 4 summarizes the results of both MIA and AIA on MIMIC-III and MIMIC-IV. The reported metrics include accuracy, precision, recall, and F1-score for MIA, as well as the AIA-F1 score. As evidenced by the results, all evaluated models—including HiSGT—exhibit an attack accuracy near 50% and low AIA-F1 scores, which confirms that the synthetic data do not reveal substantial information about individual patient membership or sensitive attributes. In particular, Table 4 reveals an inherent trade-off between fidelity and utility with privacy in synthetic EHR generation. Models such as LSTM, EVA, and SynTEG achieve the most robust privacy protection. Their MIA accuracies are around 50%—consistent with random guessing—and they report the lowest AIA-F1 scores (e.g., 0.007–0.008 on MIMIC-III), indicating that these methods leak minimal information regarding patient membership and sensitive attributes. However, this strong privacy comes at a cost: these same methods exhibit considerably lower fidelity and utility (as shown in Tables 1 and 2), meaning that their synthetic data deviate substantially from the true data distributions and present limited utility. Conversely, SOTA methods like HALO and the proposed HiSGT deliver higher fidelity and utility. When compared to HALO, HiSGT achieves similar privacy protection with an MIA F1-score of 0.472 and an AIA-F1 of 0.034 on MIMIC-III, while continuing to improve fidelity and utility.

Table 3: **Phenotype Classification Performance Across Disease Categories.** This table provides a detailed breakdown of phenotype classification performance for different disease types (acute, chronic, and mixed). We compare models trained on synthetic data (HALO and HiSGT) with real data as the ground truth. Accuracy and F1-scores are reported for each phenotype category, with macro-averaged scores included for all acute, mixed, and chronic disease groups. Results demonstrate the ability of synthetic data to support downstream predictive modeling across a diverse range of clinical conditions.

Phenotype	Type	HALO (SOTA)		HiSGT (Ours)		Real Data	
		Acc	F1-Score	Acc	F1-Score	Acc	F1-Score
Acute and unspecified renal failure	acute	0.917	0.919	0.921	0.924	0.960	0.960
Acute cerebrovascular disease	acute	0.879	0.876	0.907	0.912	0.959	0.959
Acute myocardial infarction	acute	0.887	0.890	0.917	0.919	0.952	0.953
Cardiac dysrhythmias	mixed	0.898	0.899	0.893	0.895	0.937	0.938
Chronic kidney disease	chronic	0.956	0.957	0.946	0.947	0.975	0.975
Chronic obstructive pulmonary disease	chronic	0.913	0.916	0.909	0.911	0.936	0.937
Complications of surgical/medical care	acute	0.865	0.868	0.892	0.893	0.916	0.918
Conduction disorders	mixed	0.878	0.881	0.879	0.885	0.937	0.938
Congestive heart failure; nonhypertensive	mixed	0.930	0.932	0.941	0.943	0.981	0.981
Coronary atherosclerosis and other heart disease	chronic	0.927	0.928	0.919	0.920	0.956	0.956
Diabetes mellitus with complications	mixed	0.916	0.916	0.919	0.922	0.956	0.956
Diabetes mellitus without complication	chronic	0.913	0.912	0.931	0.932	0.955	0.956
Disorders of lipid metabolism	chronic	0.916	0.917	0.923	0.926	0.963	0.963
Essential hypertension	chronic	0.946	0.946	0.939	0.940	0.957	0.958
Fluid and electrolyte disorders	acute	0.893	0.896	0.925	0.926	0.962	0.963
Gastrointestinal hemorrhage	acute	0.886	0.885	0.902	0.905	0.930	0.932
Hypertension with complications	chronic	0.941	0.941	0.939	0.940	0.977	0.977
Other liver diseases	mixed	0.875	0.877	0.892	0.891	0.946	0.947
Other lower respiratory disease	acute	0.842	0.848	0.855	0.850	0.952	0.952
Other upper respiratory disease	acute	0.749	0.723	0.767	0.770	0.923	0.924
Pleurisy; pneumothorax; pulmonary collapse	acute	0.883	0.887	0.884	0.888	0.949	0.949
Pneumonia	acute	0.880	0.885	0.896	0.899	0.942	0.944
Respiratory failure; insufficiency; arrest	acute	0.886	0.890	0.897	0.900	0.941	0.942
Septicemia (except in labor)	acute	0.913	0.914	0.923	0.924	0.974	0.974
Shock	acute	0.900	0.899	0.921	0.924	0.965	0.965
All acute diseases (macro-averaged)		0.893	0.894	0.905	0.907	0.945	0.946
All mixed diseases (macro-averaged)		0.892	0.893	0.901	0.903	0.943	0.944
All chronic diseases (macro-averaged)		0.923	0.925	0.932	0.933	0.963	0.964
All diseases (macro-averaged)		0.893	0.894	0.905	0.907	0.945	0.946

2.4 Interpretable Input Embeddings via t-SNE Visualizations

To further evaluate the ability of our model to capture meaningful hierarchical and semantic information, we perform t-SNE visualizations of input embeddings after training HiSGT and use HALO as a comparison. These visualizations help assess whether the model successfully groups medical codes into coherent clusters. From Figure 3, we observe that HALO exhibits more scattered clusters, with many points overlapping across different ICD categories. This suggests that HALO’s embedding space does not strongly enforce category-specific separation. In contrast, HiSGT demonstrates more defined and compact clusters, indicating that it captures category-level information more effectively. The improved clustering structure also leads to a more interpretable embedding space. These findings indicate that the incorporation of hierarchical and semantic representations in HiSGT enhances the clinical coherence of medical code embeddings. By preserving these relationships more effectively, HiSGT has the potential to improve fidelity and utility in synthetic EHR generation, since the generated sequences better reflect real-world clinical distributions.

Table 4: **Privacy Evaluation Results.** This table reports the performance of the membership inference attack (MIA) and attribute inference attack (AIA) on both MIMIC-III and MIMIC-IV. The metrics include accuracy, precision, recall, and F1-score for MIA, and the AIA-F1 score for AIA. An accuracy near 50% indicates that the synthetic data do not leak membership information beyond chance levels, while low AIA-F1 scores reflect robust protection against inferring sensitive attributes. Notably, the results highlight a trade-off between fidelity and utility with privacy: while models such as LSTM, EVA, and SynTEG achieve very strong privacy (evidenced by the lowest AIA-F1 scores), they suffer from poor fidelity and utility. In contrast, SOTA methods like HALO—and our proposed HiSGT—strike a better balance by delivering higher fidelity and utility with only a moderate increase in privacy risk.

Methods	MIMIC-III					MIMIC-IV				
	Acc.	Precision	Recall	F1-score	AIA-F1	Acc.	Precision	Recall	F1-score	AIA-F1
LSTM	0.500	0.500	0.494	0.497	0.008	0.507	0.507	0.502	0.505	0.011
GPT	0.504	0.504	0.462	0.482	0.036	0.511	0.512	0.480	0.495	0.044
EVA	0.500	0.500	0.462	0.480	0.007	-	-	-	-	-
SynTEG	0.509	0.510	0.482	0.495	0.007	0.516	0.517	0.484	0.500	0.022
HALO-Coarse	0.501	0.501	0.478	0.489	0.022	0.513	0.514	0.494	0.504	0.027
HALO	0.494	0.493	0.448	0.470	0.035	0.509	0.509	0.494	0.502	0.046
HiSGT (Ours)	0.493	0.492	0.454	0.472	0.034	0.504	0.504	0.478	0.491	0.045

3 Discussion

In this study, we presented HiSGT, a novel Hierarchy- and Semantics-Guided Transformer for generating synthetic EHR data with high clinical fidelity. By integrating hierarchical information from clinical coding taxonomies and semantic representations from pre-trained clinical language models, HiSGT overcomes key limitations of prior methods that treat medical codes as isolated tokens. Our extensive evaluations on the MIMIC-III and MIMIC-IV datasets demonstrate that HiSGT produces synthetic patient records that more accurately replicate real-world clinical distributions while maintaining robust privacy and competitive utility. The core fidelity metrics reveal that HiSGT substantially improves the preservation of both marginal event distributions and intra- and inter-visit dependencies compared to baseline methods. For instance, our model achieved an 8.2% improvement in the intra-visit Bigram score over HALO, indicating better capturing of the co-occurrence patterns among clinical events. These improvements are particularly important because accurate modeling of such dependencies is crucial for ensuring that synthetic data support downstream clinical applications. Further, HiSGT is a fully Transformer-based model and, contrary to HALO, does not rely on a dense

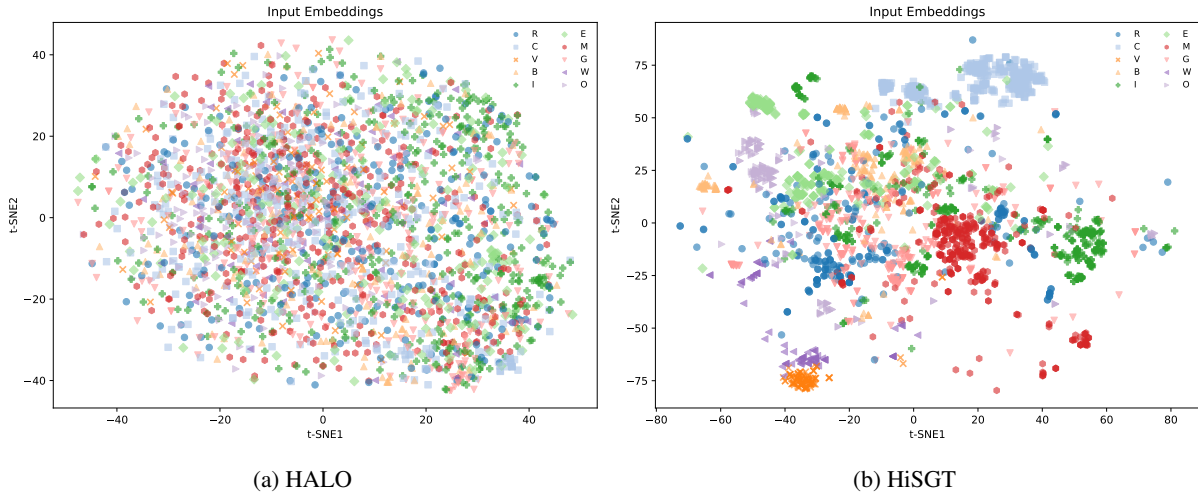


Figure 3: **t-SNE visualizations of input embeddings.** Each point represents a medical code, colored by ICD category. HALO (left) and HiSGT (right) show distinct clustering behaviors, where HALO presents more scattered clusters while HiSGT exhibits more compact and category-level clusters. The legend represents the first character of ICD chapters, e.g., ‘R’ corresponds to ‘Symptoms, signs and abnormal clinical and laboratory findings, not elsewhere classified’.

Table 5: **Ablation Study of HiSGT Components.** Each row adds a different form of embedding or consistency constraint to a base Transformer. A concurrent work, MEDTOK [Su et al., 2025], (like our variant ‘+ Hierarchy & Semantic Embs’) improves upon the code-only baseline but cannot match our full model’s fidelity, highlighting the importance of consistency regularization.

Methods	MIMIC-III				MIMIC-IV			
	Unigram	Bigram	Seq Bigram	DimWise	Unigram	Bigram	Seq Bigram	DimWise
Base (Code Only)	0.956	0.898	0.821	0.964	0.965	0.929	0.910	0.975
+ Hierarchical Emdb	0.967	0.914	0.845	0.972	0.983	0.950	0.941	0.988
+ Semantic Emdb	0.964	0.913	0.836	0.971	0.982	0.957	0.948	0.985
+ Hierarchical & Semantic Embs Similar to MEDTOK	0.976	0.927	0.859	0.984	0.987	0.960	0.953	0.989
+ Hierarchical Emdb & Consistency	0.973	0.926	0.844	0.967	0.984	0.949	0.933	0.986
+ Semantic Emdb & Consistency	0.967	0.912	0.847	0.966	0.983	0.952	0.942	0.988
+ Both Embs & Consistencies Our Full HiSGT	0.984	0.949	0.879	0.976	0.989	0.967	0.948	0.989

layer to capture intra-visit correlations (with parameters that scale quadratically with vocabulary size), making it easier to scale to very large code vocabularies. Utility evaluations further confirm that HiSGT-generated data enable the training of disease classification models that generalize well to real patient records. Although our experiments indicate that the classification performance using synthetic data is on par with SOTA baselines like HALO, HiSGT achieves this while also exhibiting higher fidelity. In our setting, the synthetic labels are generated as part of the conditional process, ensuring that the joint distribution of features and labels is preserved. This self-contained generation process minimizes the need for post-hoc label assignment and contributes to a more natural alignment between the synthetic records and their clinical interpretations. The privacy evaluation underscores a crucial trade-off between fidelity, utility, and privacy. Models such as LSTM, EVA, and SynTEG offer strong privacy protection—as evidenced by near-chance membership inference accuracy and low attribute inference F1-scores—but suffer from poor fidelity and limited utility. In contrast, HiSGT strikes an optimal balance by higher fidelity and utility with only a moderate increase in privacy risk. This balance is particularly valuable for clinical applications where preserving the nuanced relationships in patient data is as important as ensuring confidentiality. While this study focuses on integrating hierarchical and semantic representations for ICD diagnosis codes, the proposed paradigm is inherently generalizable to other medical code type including procedure and medication codes.

To evaluate the contributions of hierarchical embeddings, semantic embeddings, and consistency constraints, we conduct an ablation study (Table 5) to help analyze the different components in HiSGT. Starting with a base Transformer trained solely on medical codes, without structured knowledge, we observe that it struggles to capture co-occurrence and longitudinal dependencies. Introducing hierarchical or semantic embeddings leads to gains in all four metrics, especially Bigram and Seq Bigram. The combined use of hierarchical and semantic embeddings yields further improvements. We notice a concurrent approach, MEDTOK [Su et al., 2025], that also explores relational structure and text descriptions for medical code representations. However, its methodology differs significantly: MEDTOK trains a tokenizer with multiple loss functions to improve code embeddings for downstream tasks, whereas HiSGT not only encodes hierarchical and semantic knowledge but also enforces consistency constraints during generation. In our ablation study, the closest equivalent to MEDTOK is the ‘+ Hierarchical & Semantic Embs’ variant. While this model improves fidelity compared to a base Transformer, it remains inferior to HiSGT’s full model due to the lack of consistency regularization.

Despite these promising results, several limitations warrant further investigation. First, while HiSGT successfully integrates hierarchical and semantic information, its performance is still partially constrained by the quality and granularity of the underlying clinical ontologies and pre-trained language models. For example, even though we employ ClinicalBERT—which is pre-trained on the MIMIC dataset—it is still limited in capturing the precise semantic context. Our preliminary attempts to use contrastive learning to refine the semantic embeddings incurred significant computational overhead while yielding only marginal improvements. Future work should consider exploring alternative strategies or more domain-specific pre-training to further enhance semantic representation. Second, our utility evaluation was based on a multi-class classification paradigm for disease classification. While this task is representative, it may not fully capture the diverse clinical decision-making processes. Evaluating HiSGT on a broader range of downstream tasks—such as risk stratification or temporal event prediction—could provide a more comprehensive assessment of its clinical utility. Finally, scalability poses an important challenge. As the complexity of EHR data increases—with richer feature sets and longer patient histories—the computational cost of incorporating detailed hierarchical and semantic

representations may become prohibitive. Even after optimizing the model architecture to include the most essential embeddings and consistency regularization terms, scalability remains a potential issue. Future research should focus on optimizing training strategies and exploring more efficient model architectures to ensure that HiSGT can be applied effectively in large-scale settings.

In conclusion, our findings suggest that HiSGT represents a significant step forward in synthetic EHR data generation by balancing high clinical fidelity, robust privacy protection, and practical utility. By leveraging structured domain knowledge through hierarchical and semantic embeddings, HiSGT not only produces synthetic data that closely mirror real patient records but also facilitates downstream clinical modeling tasks. Importantly, the use of hierarchically and semantically meaningful code embeddings will also lead to more meaningful patient representations when codes are aggregated, e.g. for clustering purposes. This work opens new avenues for developing advanced synthetic data generators that can ultimately support a wide range of healthcare applications—from model benchmarking and data augmentation to collaborative research in settings where access to real patient data is limited.

4 Methods

4.1 Problem Formulation

Electronic health record data naturally exhibits a multi-level structure comprising *patients*, *visits* and *clinical events*. Let \mathcal{X} , \mathcal{V} and \mathcal{E} denote the sets of patients, visits and clinical events, respectively. For each patient $x \in \mathcal{X}$, the medical history is represented as a sequence of visits $x = \{v_1, v_2, \dots, v_{n_x}\}$, where n_x is the number of visits. Each visit v_i comprises a set of medical codes representing diagnoses, procedures, and other clinical events: $v_i = \{e_1^i, e_2^i, \dots, e_{m_i}^i\}$, with m_i denoting the number of medical codes recorded during visit v_i . The objective of synthetic EHR generation is to model the joint distribution of patient trajectories while preserving both intra-visit (within-visit) and inter-visit (longitudinal) dependencies. The model estimates the *conditional probability* of each clinical event given past visits and previously observed events within the same visit:

$$L(\Theta) = \sum_{x \in \mathcal{X}} \sum_{i=1}^{n_x} \sum_{j=1}^{m_i} \log P\left(e_j^i \mid \underbrace{v_1, \dots, v_{i-1}}_{\text{inter-visit}}, \underbrace{e_1^i, \dots, e_{j-1}^i}_{\text{intra-visit}}; \Theta\right) \quad (1)$$

where Θ represents the model parameters. The generative model seeks to maximize this likelihood to ensure that the generated sequences closely resemble real-world clinical patterns.

Once trained, a generative model can synthesize realistic EHR trajectories by predicting medical events based on past events:

$$e_j^i \sim P\left(e_j^i \mid v_1, \dots, v_{i-1}, e_1^i, \dots, e_{j-1}^i\right) \quad (2)$$

At each step j , the predicted event e_j^i is appended to the sequence, and the updated sequence is fed back into the model to generate the next event. The process continues until a predefined maximum length L is reached or an ‘END_RECORD’ token is generated, signaling the completion of a synthetic patient record.

4.2 Dataset and Baseline Details

We conduct experiments on two widely used real-world EHR datasets: **MIMIC-III** [Johnson et al., 2016] and **MIMIC-IV** [Johnson et al., 2023]. To construct patient-level longitudinal records, we first extract hospital admissions and ICD-9 diagnosis codes from both datasets. Admissions are sorted chronologically based on timestamps to maintain the correct temporal sequence of patient visits. Diagnosis codes are then aggregated at the hospital visit level, and visits are grouped by patient index, forming structured patient records that capture the progression of medical events over time. For utility evaluation, we map ICD codes to phenotype categories using a predefined benchmark taxonomy [Harutyunyan et al., 2019]. Each patient is assigned one or more phenotype labels (up to 25 labels) based on their recorded diagnoses. The dataset is then tokenized by constructing a vocabulary that includes all unique ICD codes in the dataset, 25 phenotype label tokens, and five special tokens used for sequence structuring. These special tokens: START_RECORD indicates the beginning of a patient record, END_LABEL denotes the transition from phenotype labels to visit sequences, END_VISIT marks the end of a hospital visit, END_RECORD signifies the completion of a patient record, and ‘PADDING’ ensures standardized sequence lengths. After preprocessing, MIMIC-III consists of 46,520 patients with 6,984 unique ICD diagnosis codes and 7,012 unique tokens, while MIMIC-IV includes 124,525 patients with 9,072 unique ICD codes and 9,102 unique tokens. Both datasets contain structured longitudinal patient records with multiple hospital visits, making them well-suited for evaluating synthetic EHR generation models.

To assess the effectiveness of HiSGT, we compare it against six state-of-the-art (SOTA) generative models used for EHR synthesis. LSTM [Lee, 2018] is a recurrent neural network that models sequential dependencies. GPT [Radford

et al., 2019] applies a transformer-based autoregressive approach for next-token prediction. EVA [Biswal et al., 2021] uses a variational autoencoder (VAE) to learn latent representations of EHR sequences. SynTEG [Zhang et al., 2021] employs a GAN-based framework to generate synthetic patient visits. HALO-Coarse [Theodorou et al., 2023] treats each visit as a single token, modeling longitudinal dependencies at a coarse level, while HALO [Theodorou et al., 2023] refines this approach by representing visits at a more granular level.

4.3 Experimental Setting

We conduct experiments using the MIMIC-III v1.4 and MIMIC-IV v2.2 datasets. The data is split into 80%-20% for training and testing, with an additional 90%-10% split within the training set for validation. For HiSGT, we use a six-layer Transformer architecture with eight attention heads and a hidden size of 384. Training is performed using the Adam optimizer with a learning rate of 10^{-4} , a batch size of 48, and a dropout rate of 0.1. The input sequence length is set to 768 tokens, and training is run for 100 epochs with early stopping (patience = 10) based on validation loss. The best model checkpoint is saved according to minimum validation loss. The model is implemented in Python 3.13.0 using PyTorch 2.5.0+cu121, along with scikit-learn 1.5.2, NumPy 2.1.2, and transformers 4.46.2. All experiments are conducted on a single NVIDIA H100 GPU (80GB VRAM). The HiSGT source code is publicly available at: <https://github.com/jameszhou-gl/HiSGT>.

4.4 HiSGT Framework

HiSGT is a Transformer-based generative model designed for synthetic EHR data generation. To enhance clinical fidelity, the model incorporates hierarchical and semantic embeddings to enrich medical code representations, as illustrated in Figure 1.

4.4.1 Tokenization

The tokenization process in HiSGT structures raw EHR data into a sequence of discrete tokens while preserving temporal dependencies between medical events. We extract longitudinal patient records from the MIMIC-III and MIMIC-IV datasets, using key tables such as `patients.csv`, `admissions.csv` and `diagnoses_icd.csv`. Each patient’s health timeline consists of one or more hospital visits, with each visit containing diagnosis codes that describe the patient’s conditions. To ensure an accurate representation of patient trajectories, the raw data undergoes preprocessing, where hospital visits are first sorted chronologically to maintain the correct sequence of admissions. Diagnosis codes are then grouped by patient ID, ensuring that all events for a single patient remain together. Additionally, each patient is assigned phenotype labels derived from their diagnoses, according to predefined clinical mappings. Once preprocessed, the dataset is tokenized by constructing a vocabulary that includes all unique ICD codes, along with phenotype label tokens and special tokens indicating sequence boundaries. As shown in Figure 1(a), each patient sequence follows a structured format. It begins with a `START_RECORD` token, marking the initialization of a new patient record. This is followed by phenotype label tokens that summarize the patient’s conditions, such as Hypertension with complications, Pneumonia and Chronic kidney disease. These label tokens play a crucial role in conditioning the generation of subsequent visits, ensuring consistency with standard utility evaluations. The `END_LABEL` token separates phenotype labels from individual hospital visits. Each visit is represented as a collection of medical event tokens corresponding to ICD codes, e.g., ICD9-40301 (Hypertensive chronic kidney disease) and ICD9-486 (Pneumonia, organism unspecified). To preserve temporal dependencies, events from the same visit are grouped and concluded with an `END_VISIT` token. The sequence may progress through multiple visits, maintaining the correct ordering of hospital admissions. Finally, the `END_RECORD` token indicates the end of a patient’s medical history. Since patient trajectories vary in length, `PADDING` tokens are appended where necessary to ensure consistent input dimensions.

4.4.2 Hierarchical & Semantic Embeddings

HiSGT enriches medical code representations by incorporating hierarchical and semantic embeddings, as shown in Figure 1(b). These embeddings capture structured relationships among medical codes and encode clinical meanings beyond raw code-only identifiers.

Hierarchical Embeddings. Medical coding systems such as ICD follow structured taxonomies with multiple levels of granularity, including chapter, section, category, subcategory_1, subcategory_2. For example, in ICD-10, the code ‘N18.32’ is nested within broader categories such as ‘N18.3’, ‘N18’, ‘N17-N19’ and ‘N00-N99’. To capture these relationships, we construct a hierarchical graph based on ICD-10 version $\mathcal{G} = (\mathcal{V}, \mathcal{E})$, where each node $e \in \mathcal{V}$ represents an ICD-10 code and edges $(u \rightarrow v) \in \mathcal{E}$ capture parent-child or sibling relationships extracted from the ICD ontology. This graph is represented by an adjacency matrix $A \in \{0, 1\}^{|\mathcal{V}| \times |\mathcal{V}|}$, with $A_{u,v} = 1$ if u and v share a hierarchical link.

Each code e is initially represented by an identity feature vector $\mathbf{z}_e \in \mathbb{R}^{|\mathcal{V}|}$. A graph neural network (GNN) propagates information across this hierarchy to produce clinically meaningful embeddings: $\mathbf{h}_e = \text{GNN}(\mathbf{z}_e, \mathcal{G})$, where \mathbf{h}_e is the learned hierarchical embedding for each code e . The GNN is trained using adjacency reconstruction, ensuring that embeddings for related medical codes remain close in the latent space: $\hat{A}_{u,v} = \sigma(\mathbf{h}_u^\top \mathbf{h}_v)$; where $\sigma(\cdot)$ is a sigmoid activation function. The reconstruction loss, defined as $\mathcal{L}_{\text{recon}} = \|\hat{A} - A\|$ with mean-squared error, encourages structurally related codes (e.g., ‘N18’ and ‘N18.5’) to have similar hierarchical embeddings, while unrelated codes remain distinct. The resulting hierarchical embedding \mathbf{Z}_h is then incorporated into the final input representation.

Semantic Embeddings. Beyond hierarchical relationships, medical codes are accompanied by textual descriptions that provide additional clinical context. These descriptions are essential for distinguishing between related conditions, procedures, and medications. For example, the ICD-10 code ‘E11.65’ specifies ‘Type 2 diabetes mellitus with hyperglycemia’ whereas ‘Z13.6’ specifies ‘screening for cardiovascular disorders’. Ignoring these textual descriptions can lead to synthetically generated records that fail to reflect meaningful clinical distinctions. HiSGT employs ClinicalBERT [Alsentzer et al., 2019], a pre-trained clinical language model, to encode these descriptions into dense semantic representations. Given the text description $T(e)$ corresponding to medical code e , ClinicalBERT generates a semantic embedding: $\mathbf{s}_e = \text{BERT}(T(e))$. Since ClinicalBERT outputs embeddings in a fix and high-dimensional space, we apply a linear transformation to project them into the model’s latent space: $\mathbf{Z}_s = \mathbf{W}_s \mathbf{s}_e + \mathbf{b}_s$; where $\mathbf{W}_s \in \mathbb{R}^{d_s \times d}$ and $\mathbf{b}_s \in \mathbb{R}^d$ are learnable parameters.

Final Input Representation. The final input representation \mathbf{Z} integrates three components:

$$\mathbf{Z} = \mathbf{Z}_t + \mathbf{Z}_h + \mathbf{Z}_s \quad (3)$$

Here, \mathbf{Z}_t is the standard token embedding obtained from the embedding layer in Transformer. \mathbf{Z}_h is the hierarchical embedding, derived from the GNN trained to capture relationships among medical codes. \mathbf{Z}_s is the semantic embedding, extracted from the ClinicalBERT. This enriched representation allows HiSGT to generate synthetic EHR sequences that are bot structure-aware and clinically meaningful.

4.4.3 Model Structure

HiSGT follows a decoder-only Transformer architecture [Radford et al., 2019], generating synthetic EHR sequences in an auto-regressive (AR) manner. The model processes tokenized sequences and predicts the next medical event based on prior context. As shown in Figure 1(c), the input to HiSGT consists of three components: a code token embedding \mathbf{Z}_t , a hierarchical embedding \mathbf{Z}_h , and a semantic embedding \mathbf{Z}_s . These embeddings are summed together to form the input embedding \mathbf{Z} and positional embeddings are added further to ensure the model understands the sequential nature of patient trajectories. The processed embeddings pass through six stacked Transformer decoder blocks, each comprising a masked multi-head self-attention mechanism and a feed-forward network. The attention mechanism selectively attends to relevant past events while maintaining temporal dependencies across hospital visits. A causal mask ensures that the model generates future events based only on past visits, preserving a realistic medical progression. Following the self-attention layer, the feed-forward network refines token representations through nonlinear transformations. The output of each decoder block is iteratively refined through multiple layers to progressively learn contextual dependencies. At the final stage, the hidden states of the Transformer blocks are projected onto different output heads. The next medical event in the sequence is predicted through the code head, which computes probabilities over the medical code vocabulary. To ensure that generated sequences remain clinically structured and meaningful, HiSGT introduces two additional regularization heads. The hierarchical consistency head predicts a hierarchy-aware representation, reinforcing the structured taxonomic relationships within the ICD system. The semantic consistency head maps generated medical codes back into the semantic space, ensuring that their meaning aligns with real-world clinical descriptions. While the primary objective is next-code prediction, the hierarchical and semantic consistency heads serve as essential constraints that guide the model toward more realistic and interpretable patient trajectories.

4.4.4 Training and Inference

HiSGT is trained using a multi-objective optimization approach that balances next-code prediction with hierarchical and semantic consistency constraints. The next-code prediction task is framed as a standard *cross-entropy loss*, where the model learns to predict the next code given the prior sequence of tokens. Besides, we introduce two auxiliary loss terms to ensure that generated sequences adhere to real-world medical knowledge. HiSGT employs two lightweight auxiliary heads: a hierarchy head and a semantic head. The hierarchy head maps the hidden state of each generated token back to the hierarchical embedding space, ensuring that medical codes respect their taxonomic relationships. Similarly, the semantic head projects hidden states onto the semantic embedding space, aligning generated codes with clinically meaningful representations obtained from ClinicalBERT. Both consistency objectives are formulated as *mean squared error (MSE) losses*, minimizing the discrepancy between predicted embeddings and their original input counterparts.

These auxiliary heads act as implicit regularization mechanisms, guiding the model toward generating sequences that maintain both structural coherence and semantic fidelity. Once trained, HiSGT generates synthetic patient trajectories in an AR manner. Given an initial START_RECORD token, the model first generates phenotype labels, summarizing the patient’s overall conditions. Upon detecting the special token END_LABEL, it proceeds to generate medical codes for each visit while preserving temporal dependencies. The process continues until the model outputs the END_RECORD token, marking the valid completion of a synthetic patient sequence.

4.5 Comparison of HiSGT to Related Work

EHR Data Generation. The generation of synthetic EHRs have evolved across several categories [Chen et al., 2024]. Early rule-based methods rely on predefined clinical guidelines to simulate patient records [Buczak et al., 2010, Franklin et al., 2014, McLachlan et al., 2018]. While these methods ensure clinically interpretability, they fail to capture complex correlations in real-world EHR data. GAN-based approaches model the distribution of real EHR data through adversarial training. A generator synthesizes patient records, while a discriminator distinguishes between real and synthetic samples [Zhang et al., 2020, Yale et al., 2020, Wang et al., 2024, Li et al., 2023, Baowaly et al., 2019, Yang et al., 2019, Lee et al., 2020, Yan et al., 2021, Torfi and Fox, 2020, Kuo et al., 2022]. VAE-based methods learn a latent representation of EHR data and generate new samples by sampling from the learned distribution [Biswal et al., 2021, Sun et al., 2024]. However, both of GANs and VAEs struggle with rare events in high-dimensional EHR data and capturing fine-grained longitudinal dependencies in EHR data. Recently, Transformer-based generative models gained traction due to their ability to capture long-range dependencies in patient records. HALO [Theodorou et al., 2023] applies a self-attention mechanisms to model the sequential structure of medical codes, significantly expanding the vocabulary of synthetic data from fewer than 100 tokens to over thousands. However, existing methods rely solely on modeling raw code sequences. As result, the generated records lack high clinical fidelity. In this work, we propose a Transformer-based framework with two inductive biases of hierarchical and semantic information.

Generative Transformer. The Transformer architecture, introduced by [Vaswani et al., 2017], has revolutionized sequence modeling by effectively capturing long-range dependencies through self-attention mechanisms. In natural language processing (NLP), generative Transformer models such as GPTs series [Radford et al., 2019, Brown et al., 2020] have demonstrated SOTA performance in text generation. These models predict tokens sequentially while conditioning on all previous tokens, making them highly effective for learning complex dependencies. Beyond NLP, Transformers have been successfully adapted to other domains including computer vision [Dosovitskiy et al., 2021] and multimodal learning [Hurst et al., 2024, Yang et al., 2023]. In healthcare, Transformer-based models for synthetic EHR generation typically treat patient trajectories as sequences of discrete medical codes [Theodorou et al., 2023, Pang et al., 2024]. Although they enable scaling to synthetic data with thousands of unique tokens, they model medical codes purely as discrete symbols, thereby the generated EHR lack clinical fidelity. Our work extends Transformer-based EHR generation by explicitly incorporating structured knowledge into the generative process—leveraging hierarchical representations and semantic embeddings inherent in clinical coding systems.

Additional Information

Data Availability

The MIMIC-III [Johnson et al., 2016] and MIMIC-IV [Johnson et al., 2023] electronic health record (EHR) datasets used in this study are publicly available. Access to these datasets requires completion of the necessary training and credentialing process via PhysioNet. Detailed information on obtaining access can be found at <https://physionet.org>.

Code Availability

The source code for all experiments, including dataset preprocessing, model implementation, training procedures, synthetic data generation, and evaluation, is publicly available at <https://github.com/jameszhou-gl/HiSGT>.

References

Ashish K Jha, Catherine M DesRoches, Eric G Campbell, Karen Donelan, Sowmya R Rao, Timothy G Ferris, Alexandra Shields, Sara Rosenbaum, and David Blumenthal. Use of electronic health records in us hospitals. *New England Journal of Medicine*, 360(16):1628–1638, 2009.

- Martin R Cowie, Juuso I Blomster, Lesley H Curtis, Sylvie Duclaux, Ian Ford, Fleur Fritz, Samantha Goldman, Salim Janmohamed, Jörg Kreuzer, Mark Leenay, et al. Electronic health records to facilitate clinical research. *Clinical Research in Cardiology*, 106:1–9, 2017.
- Cao Xiao and Jimeng Sun. *Introduction to deep learning for healthcare*. Springer Nature, 2021.
- Cao Xiao, Edward Choi, and Jimeng Sun. Opportunities and challenges in developing deep learning models using electronic health records data: a systematic review. *Journal of the American Medical Informatics Association*, 25(10):1419–1428, 2018.
- Alistair EW Johnson, Tom J Pollard, Lu Shen, Li-wei H Lehman, Mengling Feng, Mohammad Ghassemi, Benjamin Moody, Peter Szolovits, Leo Anthony Celi, and Roger G Mark. MIMIC-III, a freely accessible critical care database. *Scientific data*, 3(1):1–9, 2016.
- Alistair EW Johnson, Lucas Bulgarelli, Lu Shen, Alvin Gayles, Ayad Shammout, Steven Horng, Tom J Pollard, Sicheng Hao, Benjamin Moody, Brian Gow, et al. MIMIC-IV, a freely accessible electronic health record dataset. *Scientific data*, 10(1):1, 2023.
- Aldren Gonzales, Guruprabha Guruswamy, and Scott R Smith. Synthetic data in health care: A narrative review. *PLOS Digital Health*, 2(1):e0000082, 2023.
- Daniel McDuff, Theodore Curran, and Achuta Kadambi. Synthetic data in healthcare. *arXiv preprint arXiv:2304.03243*, 2023.
- Boris van Breugel, Tennison Liu, Dino Oglic, and Mihaela van der Schaar. Synthetic data in biomedicine via generative artificial intelligence. *Nature Reviews Bioengineering*, pages 1–14, 2024.
- Ghadeer O Ghosheh, Jin Li, and Tingting Zhu. A survey of generative adversarial networks for synthesizing structured electronic health records. *ACM Computing Surveys*, 56(6):1–34, 2024.
- Edward Choi, Siddharth Biswal, Bradley Malin, Jon Duke, Walter F Stewart, and Jimeng Sun. Generating multi-label discrete patient records using generative adversarial networks. In *Machine learning for healthcare conference*, pages 286–305. PMLR, 2017.
- Ziqi Zhang, Chao Yan, Thomas A Lasko, Jimeng Sun, and Bradley A Malin. Synteg: a framework for temporal structured electronic health data simulation. *Journal of the American Medical Informatics Association*, 28(3):596–604, 2021.
- Amirsina Torfi and Edward A Fox. Corgan: correlation-capturing convolutional generative adversarial networks for generating synthetic healthcare records. In *The thirty-third international flairs conference*, 2020.
- Limeng Cui, Siddharth Biswal, Lucas M Glass, Greg Lever, Jimeng Sun, and Cao Xiao. Conan: complementary pattern augmentation for rare disease detection. In *Proceedings of the AAAI conference on artificial intelligence*, volume 34, pages 614–621, 2020.
- Ziqi Zhang, Chao Yan, Diego A Mesa, Jimeng Sun, and Bradley A Malin. Ensuring electronic medical record simulation through better training, modeling, and evaluation. *Journal of the American Medical Informatics Association*, 27(1):99–108, 2020.
- Sina Rashidian, Fusheng Wang, Richard Moffitt, Victor Garcia, Anurag Dutt, Wei Chang, Vishwam Pandya, Janos Hajagos, Mary Saltz, and Joel Saltz. Smooth-gan: towards sharp and smooth synthetic ehr data generation. In *Artificial Intelligence in Medicine: 18th International Conference on Artificial Intelligence in Medicine, AIME 2020, Minneapolis, MN, USA, August 25–28, 2020, Proceedings 18*, pages 37–48. Springer, 2020.
- Nicholas I-Hsien Kuo, Mark N Polizzotto, Simon Finfer, Federico Garcia, Anders Sönnnerborg, Maurizio Zazzi, Michael Böhm, Rolf Kaiser, Louisa Jorm, and Sebastiano Barbieri. The health gym: synthetic health-related datasets for the development of reinforcement learning algorithms. *Scientific data*, 9(1):693, 2022.
- Siddharth Biswal, Soumya Ghosh, Jon Duke, Bradley Malin, Walter Stewart, Cao Xiao, and Jimeng Sun. Eva: Generating longitudinal electronic health records using conditional variational autoencoders. In *Machine Learning for Healthcare Conference*, pages 260–282. PMLR, 2021.
- Ashish Vaswani, Noam M. Shazeer, Niki Parmar, Jakob Uszkoreit, Llion Jones, Aidan N. Gomez, Lukasz Kaiser, and Illia Polosukhin. Attention is all you need. In *Neural Information Processing Systems*, 2017. URL <https://api.semanticscholar.org/CorpusID:13756489>.
- Brandon Theodorou, Cao Xiao, and Jimeng Sun. Synthesize high-dimensional longitudinal electronic health records via hierarchical autoregressive language model. *Nature communications*, 14(1):5305, 2023.
- Zeljko Kraljevic, Dan Bean, Anthony Shek, Rebecca Bendayan, Harry Hemingway, Joshua Au Yeung, Alexander Deng, Alfred Baston, Jack Ross, Esther Idowu, et al. Foresight—a generative pretrained transformer for modelling

- of patient timelines using electronic health records: a retrospective modelling study. *The Lancet Digital Health*, 6(4): e281–e290, 2024.
- Chao Pang, Xinzhuo Jiang, Nishanth Parameshwar Pavinkurve, Krishna S Kalluri, Elise L Minto, Jason Patterson, Linying Zhang, George Hripcsak, Gamze Gürsoy, Noémie Elhadad, et al. Cehr-gpt: Generating electronic health records with chronological patient timelines. *arXiv preprint arXiv:2402.04400*, 2024.
- Pawel Renc, Yugang Jia, Anthony E Samir, Jaroslaw Was, Quanzheng Li, David W Bates, and Arkadiusz Sitek. Zero shot health trajectory prediction using transformer. *NPJ Digital Medicine*, 7(1):256, 2024.
- World Health Organization et al. *International classification of diseases:[9th] ninth revision, basic tabulation list with alphabetic index*. World Health Organization, 1978.
- Emily Alsentzer, John R Murphy, Willie Boag, Wei-Hung Weng, Di Jin, Tristan Naumann, and Matthew McDermott. Publicly available clinical bert embeddings. *arXiv preprint arXiv:1904.03323*, 2019.
- Cristóbal Esteban, Stephanie L Hyland, and Gunnar Rätsch. Real-valued (medical) time series generation with recurrent conditional gans. *arXiv preprint arXiv:1706.02633*, 2017.
- Hrayr Harutyunyan, Hrant Khachatrian, David C Kale, Greg Ver Steeg, and Aram Galstyan. Multitask learning and benchmarking with clinical time series data. *Scientific data*, 6(1):96, 2019.
- Mauro Giuffrè and Dennis L Shung. Harnessing the power of synthetic data in healthcare: innovation, application, and privacy. *NPJ digital medicine*, 6(1):186, 2023.
- Xiaorui Su, Shvat Messica, Yepeng Huang, Ruth Johnson, Lukas Fesser, Shanghua Gao, Faryad Sahneh, and Marinka Zitnik. Multimodal medical code tokenizer. *arXiv preprint arXiv:2502.04397*, 2025.
- Scott H Lee. Natural language generation for electronic health records. *NPJ digital medicine*, 1(1):63, 2018.
- Alec Radford, Jeffrey Wu, Rewon Child, David Luan, Dario Amodei, Ilya Sutskever, et al. Language models are unsupervised multitask learners. *OpenAI blog*, 1(8):9, 2019.
- Xingran Chen, Zhenke Wu, Xu Shi, Hyunghoon Cho, and Bhramar Mukherjee. Generating synthetic electronic health record (ehr) data: A review with benchmarking. *arXiv preprint arXiv:2411.04281*, 2024.
- Anna L Buczak, Steven Babin, and Linda Moniz. Data-driven approach for creating synthetic electronic medical records. *BMC medical informatics and decision making*, 10:1–28, 2010.
- Jessica M Franklin, Sebastian Schneeweiss, Jennifer M Polinski, and Jeremy A Rassen. Plasmode simulation for the evaluation of pharmacoepidemiologic methods in complex healthcare databases. *Computational statistics & data analysis*, 72:219–226, 2014.
- Scott McLachlan, Kudakwashe Dube, Thomas Gallagher, Bridget Daley, Jason Walonoski, et al. The aten framework for creating the realistic synthetic electronic health record. 2018.
- Andrew Yale, Saloni Dash, Ritik Dutta, Isabelle Guyon, Adrien Pavao, and Kristin P Bennett. Generation and evaluation of privacy preserving synthetic health data. *Neurocomputing*, 416:244–255, 2020.
- Wenjie Wang, Pengfei Tang, Jian Lou, Yuanming Shao, Lance Waller, Yi-an Ko, and Li Xiong. Igamt: Privacy-preserving electronic health record synthesization with heterogeneity and irregularity. In *Proceedings of the AAAI Conference on Artificial Intelligence*, volume 38, pages 15634–15643, 2024.
- Jin Li, Benjamin J Cairns, Jingsong Li, and Tingting Zhu. Generating synthetic mixed-type longitudinal electronic health records for artificial intelligent applications. *NPJ Digital Medicine*, 6(1):98, 2023.
- Mrinal Kanti Baowaly, Chia-Ching Lin, Chao-Lin Liu, and Kuan-Ta Chen. Synthesizing electronic health records using improved generative adversarial networks. *Journal of the American Medical Informatics Association*, 26(3):228–241, 2019.
- Fan Yang, Zhongping Yu, Yunfan Liang, Xiaolu Gan, Kaibiao Lin, Quan Zou, and Yifeng Zeng. Grouped correlational generative adversarial networks for discrete electronic health records. In *2019 IEEE International Conference on Bioinformatics and Biomedicine (BIBM)*, pages 906–913. IEEE, 2019.
- Dongha Lee, Hwanjo Yu, Xiaoqian Jiang, Deevakar Rogith, Meghana Gudala, Mubeen Tejani, Qiuchen Zhang, and Li Xiong. Generating sequential electronic health records using dual adversarial autoencoder. *Journal of the American Medical Informatics Association*, 27(9):1411–1419, 2020.
- Chao Yan, Ziqi Zhang, Steve Nyemba, and Bradley A Malin. Generating electronic health records with multiple data types and constraints. In *AMIA annual symposium proceedings*, volume 2020, page 1335, 2021.
- Hongda Sun, Hongzhan Lin, and Rui Yan. Collaborative synthesis of patient records through multi-visit health state inference. In *Proceedings of the AAAI Conference on Artificial Intelligence*, volume 38, pages 19044–19052, 2024.

Tom B. Brown, Benjamin Mann, Nick Ryder, Melanie Subbiah, Jared Kaplan, Prafulla Dhariwal, Arvind Neelakantan, Pranav Shyam, Girish Sastry, Amanda Askell, Sandhini Agarwal, Ariel Herbert-Voss, Gretchen Krueger, Tom Henighan, Rewon Child, Aditya Ramesh, Daniel M. Ziegler, Jeffrey Wu, Clemens Winter, Christopher Hesse, Mark Chen, Eric Sigler, Mateusz Litwin, Scott Gray, Benjamin Chess, Jack Clark, Christopher Berner, Sam McCandlish, Alec Radford, Ilya Sutskever, and Dario Amodei. Language models are few-shot learners, 2020. URL <https://arxiv.org/abs/2005.14165>.

Alexey Dosovitskiy, Lucas Beyer, Alexander Kolesnikov, Dirk Weissenborn, Xiaohua Zhai, Thomas Unterthiner, Mostafa Dehghani, Matthias Minderer, Georg Heigold, Sylvain Gelly, Jakob Uszkoreit, and Neil Houlsby. An image is worth 16x16 words: Transformers for image recognition at scale, 2021. URL <https://arxiv.org/abs/2010.11929>.

Aaron Hurst, Adam Lerer, Adam P Goucher, Adam Perelman, Aditya Ramesh, Aidan Clark, AJ Ostrow, Akila Welihinda, Alan Hayes, Alec Radford, et al. Gpt-4o system card. *arXiv preprint arXiv:2410.21276*, 2024.

Zhengyuan Yang, Linjie Li, Kevin Lin, Jianfeng Wang, Chung-Ching Lin, Zicheng Liu, and Lijuan Wang. The dawn of lmms: Preliminary explorations with gpt-4v (ision). *arXiv preprint arXiv:2309.17421*, 9(1):1, 2023.